Numerical Scheme for the Generalised Serre-Green-Naghdi Model

1. Abstract

2. Introduction

The generalised Serre-Green-Naghdi (gSGN) equations were recently derived by Clamond and Dutykh [1], they are a set of equations that generalise the classical Serre-Green-Naghdi (SGN) first derived by Serre [2] with the addition of two parameters β_1 and β_2. The equations describe the behaviour of water waves in shallow water where the typical water depth h_0 is much smaller than the wavelength λ so that the shallowness parameter $\sigma = h_0/\lambda \ll 1$. The gSGN equations are of particular interest to the wave modelling community as their dispersion relation well approximates the dispersion relationship of the linear wave theory [3], with the choice of β values allowing for the dispersion relationship of the gSGN to be accurate up to $\mathcal{O}\left(\sigma^2\right)$ terms, $\mathcal{O}\left(\sigma^4\right)$ terms and even $\mathcal{O}\left(\sigma^6\right)$ terms [1, 4]. Therefore, these equations provide a way to study the behaviour of water waves as higher powers of σ are retained in the wave model.

In previous work we have developed and validated numerical methods for a conservative reformulation of the SGN equations [5, 6, 7, 8]. These numerical methods have all been based on the following overall scheme; firstly solve an auxiliary elliptic equation containing only spatial derivatives, to obtain all the primitive variables in the conservation equation, and then secondly evolve the remaining conservation equation using a finite volume method. The central benefit of the approach was the replication of the fundamental conservation properties of the SGN equations [8] and the robustness of the method in the presence of steep gradients [9]. The approach has been shown to produce the theoretical accuracy of the underlying methods up to third-order [7, 8] with the desired conservation and linear dispersion properties [8]. The approach has also been successfully extended to include the effects of varying bathymetry and allow for the presence of dry beds [8].

As demonstrated by Clamond and Dutykh [1], the gSGN also possesses a conservation reformulation and thus the technique described above for the SGN equations [5, 6, 7, 8] can be extended to the gSGN equations. The success of this technique for the SGN equations makes this an attractive option and would allow for an explicit, robust and conservative method for the gSGN equations with a straight forward implementation. Hence, the goal of this paper is the description of an extension to the numerical scheme of Zoppou et al. [7] for the newly developed gSGN equations [1].

This paper begins by introducing the gSGN and highlighting their important properties with regards to the developed numerical scheme. The overall numerical scheme of Zoppou et al. [7] is then described, with a straightforward second-order implementation of the method used as an example method.

This example numerical method is then validated against analytic solutions of the SGN and the Shallow Water Wave Equations (SWWE), demonstrating its convergence rate and conservation properties. Additionally, forced solutions are used to validate that all terms in the gSGN are being accurately approximated to the correct order of accuracy. Forced solutions are necessary to validate the numerical method for the more general members of this family of equations, as no analytic solutions are currently known. Together these validations demonstrate the capability of the numerical scheme to produce robust and accurate numerical methods.

3. Generalised Serre-Green-Naghdi Equations

The gSGN equations were derived by Clamond and Dutykh [1] using a Lagrangian field theory approach. These equations generalise the SGN equations that describe a depth averaged approximation to the Euler equations where $h(x,t)$ is the height of the free-surface of the water, $u(x,t)$ is the depth averaged horizontal velocity and g is the acceleration due to gravity. The gSGN equations accomplish this by introducing two free parameters β_1 and β_2, that when fixed result in a particular member of this family of equations.

The gSGN equations describe the conservation of mass (h), momentum (uh) and energy ($\mathcal{E}$) for water waves like so

$$\frac{\partial h}{\partial t} + \frac{\partial (hu)}{\partial x} = 0 \tag{1a}$$

$$\frac{\partial (hu)}{\partial t} + \frac{\partial}{\partial x}\left(hu^2 + \frac{1}{2}gh^2 + \frac{1}{2}h^2\Gamma\right) = 0 \tag{1b}$$

$$\frac{\partial (\mathcal{E})}{\partial t} + \frac{\partial}{\partial x}\left[hu\left(\frac{1}{2}u^2 + \frac{1}{4}\beta_1 h^2 \frac{\partial u}{\partial x}\frac{\partial u}{\partial x} + gh\left(1 + \frac{1}{4}\beta_2 \frac{\partial h}{\partial x}\frac{\partial h}{\partial x}\right) + \frac{1}{3}h\Gamma\right) + \frac{1}{2}\beta_2 g h^3 \frac{\partial h}{\partial x}\frac{\partial u}{\partial x}\right] = 0 \tag{1c}$$

where

$$\Gamma = \beta_1 h\left[\frac{\partial u}{\partial x}\frac{\partial u}{\partial x} - \frac{\partial^2 u}{\partial x \partial t} - u\frac{\partial^2 u}{\partial x^2}\right] - \beta_2 g\left[h\frac{\partial^2 h}{\partial x^2} + \frac{1}{2}\frac{\partial h}{\partial x}\frac{\partial h}{\partial x}\right] \tag{1d}$$

$$\mathcal{E} = \frac{1}{2}hu^2 + \frac{1}{4}\beta_1 h^3 \frac{\partial u}{\partial x}\frac{\partial u}{\partial x} + \frac{1}{2}gh^2\left(1 + \frac{1}{2}\beta_2 \frac{\partial h}{\partial x}\frac{\partial h}{\partial x}\right). \tag{1e}$$

When $\beta_1 = \beta_2 = 0$ these equations reduce to the SWWE, whilst when $\beta_1 = 2/3$ and $\beta_2 = 0$ the SGN equations are recovered.

Equation (1) holds for all β values provided the solutions are sufficiently smooth. However, for particular β values, for example those corresponding to the SWWE, it is possible to obtain non-smooth solutions for any pair of these equations that no longer satisfy all three equations simultaneously [10]. Typically, since the mass and momentum equations are solved this results in dissipation of energy around discontinuities in solutions of the SWWE.

Since (1) describes the conservation of mass, momentum and energy, when all solutions are sufficiently smooth and thus all equations hold simultaneously, the total amounts of all these quantities remain constant in time if the system is closed. This can be seen by integrating (1) over the domain, and observing that the temporal derivative of the spatial integrals of mass (h), momentum (uh) and energy ($\mathcal{E}$) is zero when there is no flux across the domain boundaries. The conservation properties of numerical solutions will be used to validate the numerical method and its solutions.

3.1. Dispersion Relation of the Linearised gSGN

The linear dispersion properties of water wave equations have been of particular interest [4, 11, 12], as the scope of wave modelling expands to include dispersive effects. Indeed, the gSGN equations are of particular interest due to their dispersion relation well approximating the dispersion relation given by the linear theory for water waves [3].

To obtain the dispersion relationship of the linearised gSGN equations, (1) is first linearised by considering small waves on a mean flow depth h_0 and mean flow velocity u_0. The dispersion relationship of the linearised gSGN equations is then obtained by seeking travelling wave solutions of the form $\exp(i(kx - \omega t))$ as was done by Zoppou et al. [7] to obtain

$$\omega^{\pm} = u_0 k \pm k\sqrt{gh_0}\sqrt{\frac{\beta_2 h_0^2 k^2 + 2}{\beta_1 h_0^2 k^2 + 2}}. \tag{2}$$

This dispersion relation provides the angular frequency ω of these travelling wave solutions of the linearised gSGN equations for waves with wavenumber k. The dispersion relation has a positive and negative branch corresponding to the direction of these waves which is denoted by the superscript on ω. This dispersion relation (2) is equivalent to the dispersion relation derived by Clamond and Dutykh [1] for the gSGN when $u_0 = 0$.

The dispersion relation of the gSGN approximates the dispersion relationship of water, as can be seen by comparing their power series approximations provided below

$$\omega^{\pm} = \left(u_0 \pm \sqrt{gh_0}\right)k \pm \frac{-1}{4}\sqrt{gh_0}k^3 h_0^2(\beta_1 - \beta_2) \pm \frac{1}{32}\sqrt{gh_0}k^5 h_0^4\left(3\beta_1^2 - 2\beta_2\beta_1 - \beta_2^2\right) + \mathcal{O}\left(k^7\right) \tag{3a}$$

$$\omega^{\pm}_{\text{water}} = u_0 k \pm \sqrt{gk\tanh(kh_0)} = \left(u_0 \pm \sqrt{gh_0}\right)k \pm \frac{-1}{6}h_0^2 k^3\sqrt{gh_0} \pm \frac{19}{360}h_0^4 k^5\sqrt{gh_0} + \mathcal{O}\left(k^7\right). \tag{3b}$$

Which is accurate up to the k term for all β values, accurate in the k^3 term when $\beta_1 = \beta_2 + 2/3$ and accurate in the k^5 term when $\beta_1 = \beta_2 + 2/3$ and $\beta_2 = 2/15$ [4]. Since $k = 2\pi/\lambda$, these power of k terms have a corresponding σ term, thus affirming the claims in the introduction. Since the β values allow us to alter the accuracy of the dispersion relationship the gSGN equations allows us to consistently compare the effect of the dispersion relationship on numerical solutions and thus physical phenomena.

From the dispersion relation (2), the phase speed v_p and the group speed v_g can be derived as follows

$$v_p^{\pm} = \frac{\omega^{\pm}}{k} = u_0 \pm \sqrt{gh_0}\sqrt{\frac{\beta_2 h_0^2 k^2 + 2}{\beta_1 h_0^2 k^2 + 2}}, \tag{4a}$$

$$v_g^{\pm} = \frac{\partial \omega^{\pm}}{\partial k} = u_0 \pm \sqrt{gh_0}\sqrt{\frac{\beta_2 h_0^2 k^2 + 2}{\beta_1 h_0^2 k^2 + 2}}\left[1 + \frac{\beta_2 - \beta_1}{\left(\frac{1}{2}\beta_2 h_0^2 k^2 + 1\right)\left(\left(\beta_1 - \frac{1}{3}\right) h_0^2 k^2 + 1\right)}\right]. \tag{4b}$$

3.1.1. Phase Speed Bounds

Using phase speed bounds of the SGN equations Le Métayer et al. [13] and Zoppou et al. [7] applied approximate Riemann solvers such as those of Kurganov et al. [14] to solve the SGN. Thus, if the gSGN can also be shown to have bounded phase speeds then similar methods can be applied to solve the gSGN.

To demonstrate that the phase speeds are bounded, observe that when $\beta_1 \geq 0$, $\beta_2 \geq 0$ and $h_0 k \geq 0$ then

$$f(h_0 k) = \frac{\beta_2 \left(h_0 k\right)^2 + 2}{\beta_1 \left(h_0 k\right)^2 + 2},$$

is a monotone function over $h_0 k$. This can be seen by reformulating and taking the derivative with respect to $h_0 k$, to obtain that

$$\frac{\partial \left(f(h_0 k)\right)}{\partial \left(h_0 k\right)} = \left[\frac{\beta_2}{\beta_1} - 1\right] \frac{4\left(h_0 k\right)}{\beta_1 \left(\frac{4}{\beta_1} + \left(h_0 k\right)^2\right)^2}.$$

The derivative is greater than 0 and thus monotone non-increasing if $\beta_2 \leq \beta_1$ and less than 0 and thus monotone non-decreasing if $\beta_2 \geq \beta_1$ given the initial assumptions. Since $v_p^+ = u_0 + \sqrt{gh_0 f(h_0 k)}$ and $v_p^- = u_0 - \sqrt{gh_0 f(h_0 k)}$, given the above properties of $f(h_0 k)$ under the initial assumptions v_p^+ is monotone non-decreasing and v_p^- is monotone non-increasing when $\beta_2 \leq \beta_1$ and v_p^+ is monotone non-increasing and v_p^- is monotone non-decreasing when $\beta_2 \geq \beta_1$.

In addition to the monotonicity of $v_p^{\pm}$ when $k \to 0$ then $v_p^{\pm} \to u_0 \pm \sqrt{gh_0}$ whilst as $k \to \infty$ then $v_p^{\pm} \to u_0 \pm \sqrt{gh_0}\sqrt{\beta_2/\beta_1}$. Therefore, $v_p^{\pm}$ is monotonic and bounded at the limits of the domain, and thus bounded for all β values provided that $\beta_1 = 0$ only when $\beta_2 = 0$, otherwise the $k \to \infty$ limit, is no longer bounded. Therefore, the methods of Le Métayer et al. [13] and Zoppou et al. [7] for the SGN equations can be extended to the gSGN as phase speeds are bounded.

In addition to the phase speed bounds we also have the following chain of inequalities when $\beta_2 \leq \beta_1$

$$u_0 - \sqrt{gh_0} \leq v_p^- \leq u_0 - \sqrt{gh_0}\sqrt{\frac{\beta_2}{\beta_1}} \leq u_0 \leq u_0 + \sqrt{gh_0}\sqrt{\frac{\beta_2}{\beta_1}} \leq v_p^+ \leq u_0 + \sqrt{gh_0}. \tag{5}$$

We designate this region of β values, as 'Region 1', it is characterised by either lack of dispersion when $\beta_2 = \beta_1$ or trailing dispersive waves when $\beta_2 < \beta_1$. Region 1 includes the SWWE and the SGN and is consistent with the behaviour of the dispersion given by the linear theory for water waves [3].

When $\beta_2 > \beta_1$ the inequality chain becomes

$$u_0 - \sqrt{gh_0}\sqrt{\frac{\beta_2}{\beta_1}} \leq v_p^- \leq u_0 - \sqrt{gh_0} \leq u_0 \leq u_0 + \sqrt{gh_0} \leq v_p^+ \leq u_0 + \sqrt{gh_0}\sqrt{\frac{\beta_2}{\beta_1}} \tag{6}$$

This will be denoted as 'Region 2', it is characterised by advancing dispersive waves. Advancing dispersive waves are not observed for water waves, and thus none of the equations or family of equations of interest lie

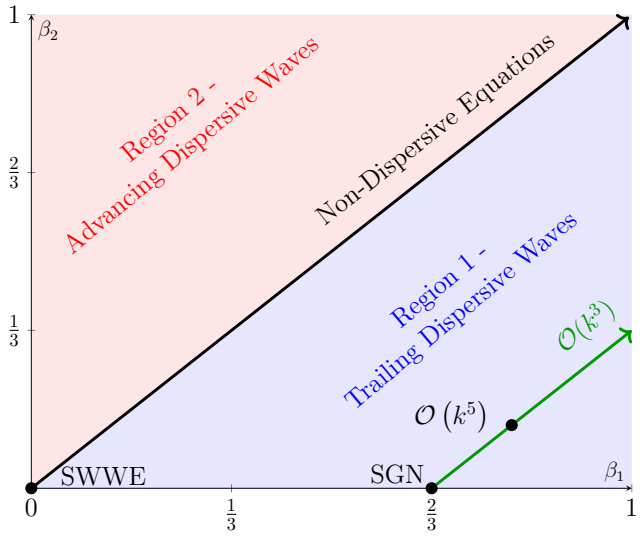

Figure 1: Phase speed regions of gSGN in terms of β_1 and β_2 showing important equations and labelling combinations of β and their associated dispersion relationship accuracy.

in this region. Hence, the study in this paper will be restricted to Region 1, although the numerical scheme is valid for both regions.

The regions and location of important members in terms of β values is summarised in Figure 1. Additionally, this figure also demonstrates the accuracy of the dispersion relationship of the gSGN compared to the dispersion relation given by the linear theory for water waves (3).

3.2. Alternative Conservative Form of the gSGN

Clamond and Dutykh [1] demonstrated a rearrangement of (1b) for the gSGN, in an analogous way to the reformulations of SGN [7, 13, 15]. The purpose of this reformulation is to remove the mixed spatial-temporal derivative in the flux term, which is difficult to treat numerically. This reformulation is obtained by introducing a new conserved quantity G

$$G = hu - \frac{\beta_1}{2}\frac{\partial}{\partial x}\left(h^3\frac{\partial u}{\partial x}\right)$$

and thus (1b) can be written in conservation law form for G as

$$\frac{\partial G}{\partial t} + \frac{\partial}{\partial x}\left(uG + \frac{gh^2}{2} - \beta_1 h^3 \frac{\partial u}{\partial x}\frac{\partial u}{\partial x} - \frac{1}{2}\beta_2 g h^2\left[h\frac{\partial^2 h}{\partial x^2} + \frac{1}{2}\frac{\partial h}{\partial x}\frac{\partial h}{\partial x}\right]\right) = 0$$

When $\beta_1 = 2/3$ then G is the same conserved quantity introduced for the SGN equations [7, 13, 15].

This reformulation, provides the gSGN equations in conservation law form for both h and the new conserved quantity G. Thus the conservative gSGN equations are

$$\frac{\partial h}{\partial t} + \frac{\partial (uh)}{\partial x} = 0 \tag{7a}$$

$$\frac{\partial G}{\partial t} + \frac{\partial}{\partial x}\left(uG + \frac{gh^2}{2} - \beta_1 h^3 \frac{\partial u}{\partial x}\frac{\partial u}{\partial x} - \frac{1}{2}\beta_2 g h^2\left[h\frac{\partial^2 h}{\partial x^2} + \frac{1}{2}\frac{\partial h}{\partial x}\frac{\partial h}{\partial x}\right]\right) = 0. \tag{7b}$$

with

$$G = uh - \frac{\beta_1}{2}\frac{\partial}{\partial x}\left(h^3\frac{\partial u}{\partial x}\right). \tag{7c}$$

Now that the gSGN equations are written in conservation law form and have a bound on the phase speeds, they can be solved numerically using the hybrid finite volume technique described by Zoppou et al. [7].

4. Numerical Scheme

The proposed numerical scheme for the gSGN extends those previously published for the SGN equations [7, 13] to allow any β values and the associated additional terms. We begin the description of the numerical scheme by giving a brief outline of the finite volume method and the discretisation therein. We then provide an overview of the numerical technique and then describe the simplest second-order implementation of this scheme in detail. With previous studies [7, 8] showing the sufficiency and necessity of second-order methods for the SGN equations.

4.1. Finite Volume Method and Discretisation

The heart of these hybrid finite volume methods for the gSGN equations is the finite volume method used to solve the equations in conservation law form. The finite volume method solves equations of the form

$$\frac{\partial q}{\partial t} + \frac{\partial}{\partial x}\left[f(q)\right] = 0 \tag{8}$$

where q is a generic quantity. This is the form of the gSGN equations after the reformulation (7). The finite volume method does this by integrating (8) across cells of fixed width Δx in space and over time steps of fixed length Δt. The midpoint of the j^{th} cell is given by $x_j = x_0 + j\Delta x$ while the cell edges of the j^{th} cell are given by $x_{j-1/2} = x_0 + (j - \frac{1}{2})\Delta x$ and $x_{j+1/2} = x_0 + (j + \frac{1}{2})\Delta x$. Likewise the n^{th} time step is given by $t^n = t^0 + n\Delta t$.

Integrating (8) over both space and time one results in

$$\bar{q}_j^{n+1} = \bar{q}_j^n + \frac{\Delta t}{\Delta x}\left[F_{j+1/2}^n - F_{j-1/2}^n\right] \tag{9}$$

where

$$\bar{q}_j^n = \frac{1}{\Delta x}\int_{x_j-\Delta x/2}^{x_j-\Delta x/2} q(x, t^n)\, dx$$

is the average of q over the j^{th} cell at time t^n and

$$F_{j\pm1/2}^n = \frac{1}{\Delta t}\int_{t^n}^{t^{n+1}} f(q(x_{j\pm1/2}, t))dt$$

is the average flux of q across the cell edge from time t^n to t^{n+1}. Therefore, if $F_{j\pm1/2}^n$ can be approximated with the appropriate order of accuracy, then we have an explicit method for updating the cell average of the conserved quantities through time for equations in conservation law form (8).

4.2. Overview

Since the core of this numerical scheme is the finite volume method, we will continue the discretisation used above. Additionally, when describing this broad overview it is also useful to consider collections of the point-wise or cell averaged values described above over the whole domain at a particular time. Thus for an generic quantity q, we define $\boldsymbol{q}^n$ to be the vector of q_j^n values and $\bar{\boldsymbol{q}}^n$ to be the vector of $\bar{q}_j^n$ values for all cells in the domain at time t^n.

The numerical scheme for the gSGN equations based on the finite volume method (9) then proceeds as follows by beginning at a generic n^{th} time step

1. Begin with the vectors of cell averages of the conserved quantities $\bar{\boldsymbol{h}}^n$ and $\bar{\boldsymbol{G}}^n$.
2. Solve (7c) using $\bar{\boldsymbol{h}}^n$ and $\bar{\boldsymbol{G}}^n$ to obtain an approximation to $\bar{\boldsymbol{u}}^n$, which can be written
$$\mathcal{A}\left(\bar{\boldsymbol{h}}^n, \bar{\boldsymbol{G}}^n\right) = \bar{\boldsymbol{u}}^n.$$
3. Solve (7b) and (7a) using the finite volume method (9) with the approximate Riemann solver of Kurganov et al. [14] to obtain $\bar{h}_j^{n+1}$ and $\bar{G}_j^{n+1}$ at the next time step, like so
$$\mathcal{F}\left(\bar{\boldsymbol{h}}^n, \bar{\boldsymbol{G}}^n, \bar{\boldsymbol{u}}^n\right) = \bar{\boldsymbol{h}}^{n+1}, \bar{\boldsymbol{G}}^{n+1}.$$
4. However, since $\mathcal{F}$ is only first order accurate in time, Steps 1-3 are repeated and then appropriate order approximations to $\bar{\boldsymbol{h}}^{n+1}$,$\bar{\boldsymbol{G}}^{n+1}$ are obtained using a SSP Runge Kutta method [16].

This numerical scheme produces the numerical methods of Le Métayer et al. [13], Zoppou et al. [7] and Pitt [8] when $\beta_1 = 2/3$ and $\beta_2 = 0$. Additionally, when $\beta_1 = \beta_2 = 0$ the gSGN reduces to the SWWE, and this numerical scheme reduces to a finite volume method [17].

4.3. Example Implementation

To demonstrate the utility of this numerical scheme we present a simple second-order implementation, and then validate it in the following section. The description of this numerical method will be broken up into the above steps for simplicity and also to highlight the interchangeability of the different parts of the scheme.

4.3.1. Step 2 - Solution of Elliptic Equation

To solve (7c) with $\bar{\boldsymbol{h}}^n$ and $\bar{\boldsymbol{G}}^n$ to obtain $\bar{\boldsymbol{u}}^n$ we use the observation that the cell average and the cell nodal value are approximately equal with second-order accuracy so that $\bar{\boldsymbol{q}}^n = \boldsymbol{q}^n + \mathcal{O}\left(\Delta x^2\right)$ for all the quantities of interest. The second-order central finite difference approximation to (7c) can then be written as

$$\boldsymbol{u}^n = \boldsymbol{A}^{-1}\boldsymbol{G}^n \tag{10}$$

where $\boldsymbol{A}$ is a tri-diagonal matrix where the sub-diagonal, diagonal and super-diagonal are given by

$$\begin{aligned}
A_{j,j-1} &= -\frac{\beta_1}{2}\left[\frac{\left(h_j^n\right)^3}{\Delta x^2} - \frac{3\left(h_j^n\right)^2}{2\Delta x}\frac{h_{j+1}^n - h_{j-1}^n}{2\Delta x}\right] \\
A_{j,j} &= h_j^n + \beta_1\frac{\left(h_j^n\right)^3}{\Delta x^2} \\
A_{j,j+1} &= -\frac{\beta_1}{2}\left[\frac{\left(h_j^n\right)^3}{\Delta x^2} + \frac{3\left(h_j^n\right)^2}{2\Delta x}\frac{h_{j+1}^n - h_{j-1}^n}{2\Delta x}\right]
\end{aligned}$$

with all other elements in $\boldsymbol{A}$ being zero.

The finite difference approximation (10) can be solved with any matrix solver, for this method we use the explicit Thomas Algorithm [18]. This is a good method as long as the diagonals are strictly greater than zero which is the case as long as $h_j^n > 0$, which is true for all the problems of interest in this paper.

Thus as desired we have

$$\mathcal{A}\left(\bar{\boldsymbol{h}}^n, \bar{\boldsymbol{G}}^n\right) = \boldsymbol{A}^{-1}\boldsymbol{G}^n = \boldsymbol{u}^n = \bar{\boldsymbol{u}}^n. \tag{11}$$

4.3.2. Reconstruction of quantities at cell boundaries

The finite volume method of Kurganov et al. [14] relies on approximations of all the terms in the spatial derivative at the cell edges $x_{j\pm1/2}$. Thus the following quantities require second-order approximations at the cell edges: u, h, G, $\partial u/\partial x$, $\partial h/\partial x$, $\partial^2 h/\partial x^2$. In this paper we are interested in reproducing solutions to either smooth analytic and forced solutions or the discontinuous dam-break solutions of the SWWE where only h, u and G need to be approximated. For this reason our approximations to to u, h, G, will allow for discontinuities and thus use limiting while the approximations to the derivatives $\partial u/\partial x$, $\partial h/\partial x$, $\partial^2 h/\partial x^2$ will assume that these quantities are smooth and thus do not require limiting.

For h, u and G to get a second-order approximation that ensures stability in the presence of discontinuities we employ slope limiting, as done previously for the SGN equations [7]. The reconstructions for all these quantities can be summarised for a general quantity q like so

$$q_{j-1/2}^+ = \bar{q}_j - \frac{\Delta x}{2}s_j \qquad \text{and} \qquad q_{j-1/2}^- = \bar{q}_j + \frac{\Delta x}{2}s_j \tag{12}$$

where

$$s_j = \text{minmod}\left(\theta\frac{\bar{q}_j - \bar{q}_{j-1}}{\Delta x}, \frac{\bar{q}_{j+1} - \bar{q}_{j-1}}{2\Delta x}, \theta\frac{\bar{q}_{j+1} - \bar{q}_j}{\Delta x}\right). \tag{13}$$

The minmod function is defined as follows

$$\text{minmod}\left(a,b,c\right) = \begin{cases} \min\left(a,b,c\right) & \text{when} \quad a<0, b<0, c<0 \\ \max\left(a,b,c\right) & \text{when} \quad a>0, b>0, c>0 \\ 0 & \text{otherwise} \end{cases}. \tag{14}$$

This gives a reconstruction at the cell level for each cell edge, so cell j gives rise to $q_{j-1/2}^+$ and $q_{j+1/2}^-$ while cell $j+1$ gives rise to $q_{j+1/2}^+$ and $q_{j+3/2}^-$ all of which are required by the flux approximation.

For $\partial u/\partial x$, $\partial h/\partial x$ and $\partial^2 h/\partial x^2$ we assume that the quantities are smooth, and so using the appropriate order finite difference approximation at the cell edges is sufficient. We demonstrate this for cell $x_{j+1/2}$ and a general quantity q

$$\left[\frac{\partial q}{\partial x}\right]_{j+1/2} = \frac{q_{j+1} - q_j}{\Delta x},$$
$$\left[\frac{\partial^2 q}{\partial x^2}\right]_{j+1/2} = \frac{q_{j+2} - q_{j+1} - q_j + q_{j-1}}{2\Delta x^2}.$$

4.3.3. Step 3 - Finite Volume Method

To solve (7b) and (7a) which are both in conservation law form (8) we use (9). Since we begin with $\bar{\boldsymbol{h}}^n$ and $\bar{\boldsymbol{G}}^n$, we only require an approximation to $F^n_{j\pm1/2}$ to make use of (9) to obtain $\bar{\boldsymbol{h}}^{n+1}$ and $\bar{\boldsymbol{G}}^{n+1}$.

In this numerical scheme the flux approximation method described by Kurganov et al. [14] for $F^n_{j\pm1/2}$ is used. This central benefit of this scheme is that it only requires bounds on the phase speeds. Only the calculation of the flux term $F^n_{j+1/2}$ is demonstrated as the process to calculate the flux term $F^n_{j-1/2}$ is identical but with different cells. For a general quantity q the flux approximation method [14] is

$$F^n_{j+\frac{1}{2}} = \frac{a^+_{j+\frac{1}{2}} f\left(q^-_{j+\frac{1}{2}}\right) - a^-_{j+\frac{1}{2}} f\left(q^+_{j+\frac{1}{2}}\right)}{a^+_{j+\frac{1}{2}} - a^-_{j+\frac{1}{2}}} + \frac{a^+_{j+\frac{1}{2}}\, a^-_{j+\frac{1}{2}}}{a^+_{j+\frac{1}{2}} - a^-_{j+\frac{1}{2}}}\left[q^+_{j+\frac{1}{2}} - q^-_{j+\frac{1}{2}}\right] \tag{15}$$

where $a^+_{j+\frac{1}{2}}$ and $a^-_{j+\frac{1}{2}}$ are given by the phase speed bounds and all quantities on the right hand side are computed at time t^n. Applying the phase speed bounds (5) and (6) we obtain

$$a^-_{j+\frac{1}{2}} = \min\left\{0\ ,\ u^-_{j+1/2} - \max\left(1, \sqrt{\frac{\beta_2}{\beta_1}}\right)\sqrt{gh^-_{j+1/2}}\ ,\ u^+_{j+1/2} - \max\left(1, \sqrt{\frac{\beta_2}{\beta_1}}\right)\sqrt{gh^+_{j+1/2}}\right\}, \tag{16}$$

$$a^+_{j+\frac{1}{2}} = \max\left\{0\ ,\ u^-_{j+1/2} + \max\left(1, \sqrt{\frac{\beta_2}{\beta_1}}\right)\sqrt{gh^-_{j+1/2}}\ ,\ u^+_{j+1/2} + \max\left(1, \sqrt{\frac{\beta_2}{\beta_1}}\right)\sqrt{gh^+_{j+1/2}}\right\} \tag{17}$$

where the $\max\left(1, \sqrt{\frac{\beta_2}{\beta_1}}\right)$ accounts for the different phase speed bounds (5) and (6) which depend on the choice of β values.

The flux functions $f(q^-_{j+\frac{1}{2}})$ and $f(q^+_{j+\frac{1}{2}})$ are evaluated using the reconstructed values of the j^{th} and $(j+1)^{th}$ cell respectively. From the continuity equation (7b) we have

$$f\left(h^\pm_{j+\frac{1}{2}}\right) = u^\pm_{j+1/2} h^\pm_{j+1/2}.$$

For the evolution of G equation (7a) we have

$$f\left(G^\pm_{j+\frac{1}{2}}\right) = u^\pm_{j+1/2} G^\pm_{j+1/2} + \frac{g}{2}\left(h^\pm_{j+1/2}\right)^2 - \beta_1\left(h^\pm_{j+1/2}\right)^3\left(\left[\frac{\partial u}{\partial x}\right]_{j+1/2}\right)^2$$
$$- \frac{1}{2}\beta_2 g\left(h^\pm_{j+1/2}\right)^2\left[h^\pm_{j+1/2}\left[\frac{\partial^2 h}{\partial x^2}\right]_{j+1/2} + \frac{1}{2}\left(\left[\frac{\partial h}{\partial x}\right]_{j+1/2}\right)^2\right]. \tag{18}$$

where derivatives are assumed to be smooth over the cell edge, and thus do not require different superscripts.

Since the reconstructions were given above for all these quantities, we can approximate $F^n_{j\pm1/2}$ using (15) and thus employ (9) to obtain $\bar{\boldsymbol{h}}^{n+1}$ and $\bar{\boldsymbol{G}}^{n+1}$ resulting in

$$\mathcal{F}\left(\bar{\boldsymbol{h}}^n, \bar{\boldsymbol{G}}^n, \bar{\boldsymbol{u}}^n\right) = \bar{q}^n_j + \frac{\Delta t}{\Delta x}\left[F^n_{j+1/2} - F^n_{j-1/2}\right] = \bar{\boldsymbol{h}}^{n+1}, \bar{\boldsymbol{G}}^{n+1} \tag{19}$$

as desired.

4.3.4. Step 4 - Runge-Kutta Time Stepping

Combining both Steps 2 and Steps 3, provides a spatially second-order scheme with first-order time stepping. To arrive at a fully second-order method, we make use of repeating Steps 2 and Steps 3 and applying the second-order SSP Runge Kutta method [16]. Doing this we obtain the following scheme making use of the above implementation of $\mathcal{A}$ (11) and $\mathcal{F}$ (19)

$$\begin{aligned}\bar{\boldsymbol{h}}^{'}, \bar{\boldsymbol{G}}^{'} &= \mathcal{F}\left(\bar{\boldsymbol{h}}^{n}, \bar{\boldsymbol{G}}^{n}, \mathcal{A}\left(\bar{\boldsymbol{h}}^{n}, \bar{\boldsymbol{G}}^{n}\right)\right)\\ \bar{\boldsymbol{h}}^{''}, \bar{\boldsymbol{G}}^{''} &= \mathcal{F}\left(\bar{\boldsymbol{h}}^{'}, \bar{\boldsymbol{G}}^{'}, \mathcal{A}\left(\bar{\boldsymbol{h}}^{'}, \bar{\boldsymbol{G}}^{'}\right)\right)\\ \bar{\boldsymbol{h}}^{n+1}, \bar{\boldsymbol{G}}^{n+1} &= \frac{1}{2}\left(\bar{\boldsymbol{h}}^{n} + \bar{\boldsymbol{h}}^{''}\right), \frac{1}{2}\left(\bar{\boldsymbol{G}}^{n} + \bar{\boldsymbol{G}}^{''}\right).\end{aligned}$$

Hence we obtain a stable fully second-order method.

4.4. Boundary Conditions

For the purposes of the validation below and for simplicity, we have applied Dirichlet boundary conditions using ghost cells over which the values of h, G and u are completely determined. Thus in addition to the m cells inside the boundary we have an additional l cells either side of it so that we have the left ghost cells $-l$, $-l+1, \ldots, -1$ and the right ghost cells m, $m+1, \ldots, m+l-1$. Since the example numerical method has a maximum stencil that extends 2 cells beyond the target cell, then l must be at least 2.

This boundary condition is applied to Step 2 by extending the matrix equation (10) to vectors containing the ghost cells $\hat{\boldsymbol{u}}^n$ and $\hat{\boldsymbol{G}}^n$ like so

$$\hat{\boldsymbol{u}}^n = \begin{bmatrix} u^n_{-l} & \ldots & u^n_{-1} & u^n_0 & \ldots & u^n_{m-1} & u^n_m & \ldots & u^n_{m+l-1}\end{bmatrix}^T \tag{20}$$

$$\hat{\boldsymbol{G}}^n = \begin{bmatrix} G^n_{-l} & \ldots & G^n_{-1} & G^n_0 & \ldots & G^n_{m-1} & G^n_m & \ldots & G^n_{m+l-1}\end{bmatrix}^T. \tag{21}$$

Likewise the associated extended matrix $\hat{\boldsymbol{A}}$ in (10) is the same as $\boldsymbol{A}$ when $0 \geq j \leq m$ defined above with the additional associated ghost cell values given by

$$\hat{A}_{j,j-1} = 0 \qquad \hat{A}_{j,j} = 1 \qquad \hat{A}_{j,j+1} = 0 \tag{22}$$

when $j < 0$ or $j > m-1$.

For Step 3, since the ghost cells contain the complete representation of h, G and u over them, there is no need to reconstruct the quantities inside the ghost cells.

4.5. Courant-Frederichs-Lewy Condition

To ensure the stability of the finite volume method (9) the Courant-Friedrichs-Lewy (CFL) condition [19] is used. The CFL condition is necessary for stability and ensures that time steps are small enough so that information is only transferred between neighbouring cells. For the gSGN equations the CFL condition is

$$\Delta t \leq \frac{Cr}{\max_j\left\{a^{\pm}_{j+1/2}\right\}}\Delta x \tag{23}$$

where $a^{\pm}_{j+1/2}$ are the phase speed bounds used in the flux approximation (17) and $0 \leq Cr \leq 1$ is the Courant number.

5. Validation

The example numerical method described above is validated using analytic solutions for particular β values that correspond to the SGN equations and the SWWE and a forced solution. Together these tests demonstrate the ability of the method to reproduce analytic solutions to important members of the gSGN family, as well as solve the gSGN for any pair of β values that admit phase speed bounds.

5.1. Convergence and Conservation Measures

To validate that the produced numerical solutions we make use of measures of convergence and conservation. The measure of convergence will be the distance between the numerical solution and the equivalent analytic or forced solution using the L_2 norm. While the conservation properties of the numerical method will be measured by numerically approximating the energy in the initial conditions and the numerical solution and comparing them using a measure called C_1.

For a quantity q with a vector of its analytic or forced solution at the cell midpoints $\boldsymbol{q}$ and the numerical solution at the cell midpoints $\boldsymbol{q}^*$, the discrete L_2 norm is

$$L_2\left(\boldsymbol{q}, \boldsymbol{q}^*\right) = \sqrt{\frac{\sum_{j=0}\left[q_j^2 - \left(q_j^*\right)^2\right]}{\sum_{j=0}\left[q_j^2\right]}} \tag{24}$$

where the time-step superscripts were suppressed for simplicity.

For a quantity q with a vector of its values at the n^{th} time step $\boldsymbol{q}^n$, the total amount of the quantity is approximated by $C(\boldsymbol{q}^n)$. The method for this is the same as the method described by Zoppou et al. [7], which has a higher order of accuracy than the numerical method it is measuring. Using the numerical approximation to the total amounts, the conservation error is obtained in the following way

$$C_1\left(\boldsymbol{q}^0, \boldsymbol{q}^n\right) = \begin{cases} \dfrac{\left|C(\boldsymbol{q}^0) - C(\boldsymbol{q}^n)\right|}{\left|C(\boldsymbol{q}^0)\right|} & , \quad \left|C(\boldsymbol{q}^0)\right| > 0 \\ \left|C(\boldsymbol{q}^0) - C(\boldsymbol{q}^n)\right| & , \quad \left|C(\boldsymbol{q}^0)\right| = 0 \end{cases} . \tag{25}$$

- Analytic solutions - we recover them (conservation and norm)
- Forced solutions - our numerical method can handle any combination of beta values, all terms are approximated with correct order of accuracy. Limiters on gradients off.

5.2. Analytic Solutions

The analytic solutions used to validate the numerical method, are the solitary travelling wave solution of the SGN equations and the dam-break solution of the SWWE. The soliton solution is a smooth travelling wave solution, that assesses the balance of the non-linear and dispersive terms in the gSGN equations. Whereas the dam-break solution of the SWWE demonstrates the robustness of the method in the presence of steep gradients. The soliton solution used in this paper, is the same as the soliton solution used for validation by Pitt [8], allowing for a comparison of this gSGN solver to the more specialised SGN solvers described therein.

5.2.1. Serre Equations ($\beta_1 = 2/3$ and $\beta_2 = 0$) - Solitary Travelling Wave Solution

When $\beta_1 = 2/3$ and $\beta_2 = 0$ the gSGN equations are equivalent to the SGN equations which admit the following travelling wave solution [20]

$$h(x,t) = a_0 + a_1 \mathrm{sech}^2\left(\kappa(x - ct)\right), \tag{26a}$$

$$u(x,t) = c\left(1 - \frac{a_0}{h(x,t)}\right), \tag{26b}$$

where

$$\kappa = \frac{\sqrt{3a_1}}{2a_0\sqrt{a_0 + a_1}} \tag{26c}$$

and

$$c = \sqrt{g\left(a_0 + a_1\right)}. \tag{26d}$$

This travelling wave solution is maintained due to a balance between the dispersive terms and the non-linear terms in the momentum equation (3.2). Validating the numerical solutions for the gSGN solver using this solution tests the balance between these terms in (3.2), and allows us to verify the method's conservation of energy as the solution is smooth. To enable a comparison between the numerical method and the SGN solver

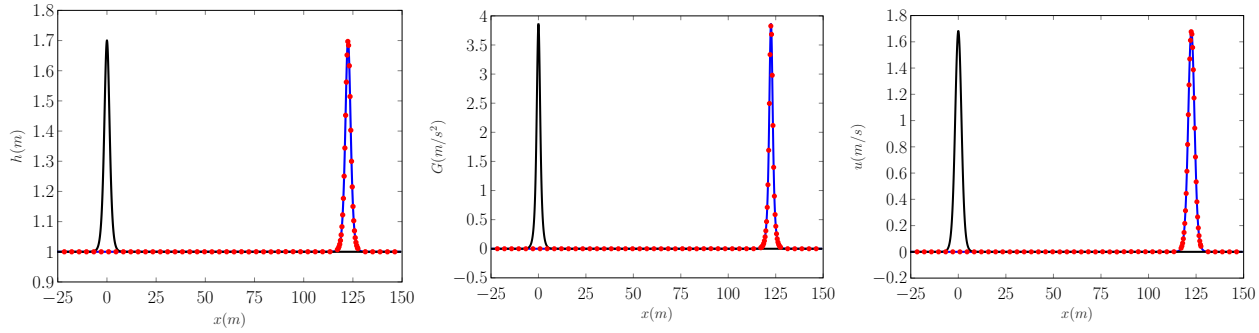

(a) h (b) G (c) u

Figure 2: Plot of comparing initial (—), analytic solution (—), and numerical solution with $\Delta x \approx 0.06m$ (●) at $t = 30s$.

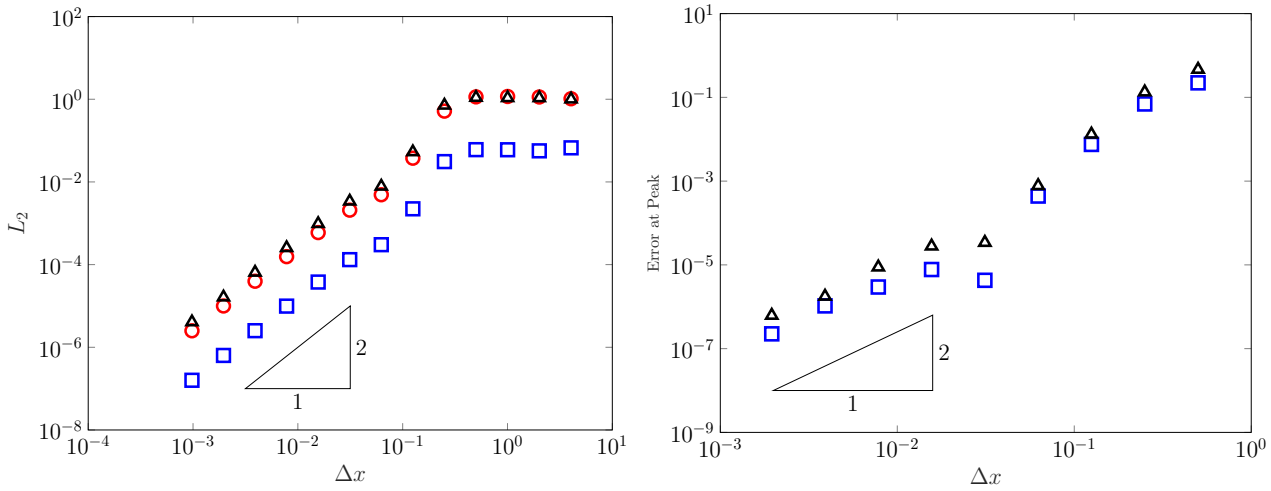

(a) L_2 (b) Convergence to peak values

Figure 3: Convergence plots for h (□) , G (○) and u (△) as Δx varies.

of Zoppou et al. [7] the chosen soliton parameters were $a_0 = 1m$ and $a_1 = 0.7m$ and the acceleration due to gravity at the earth surface, $g = 9.81m^2/s$ was used.

The numerical solution was solved over the domain $[-200m, 200m]$ from $t = 0s$ until $t = 30s$. To ensure that the SGN solution is recovered, $\beta_1 = 2/3$ and $\beta_2 = 0$. The spatial resolution was varied like so $\Delta x = 400/(100 \times 2^l)$, where l was increased from 0 to 12. To satisfy the CFL condition (23) the time step width $\Delta t = \Delta x/(2\sqrt{g(a_0 + a_1)})$ [8] was chosen. The limiting parameter θ was set to $\theta = 1.2$, matching the numerical experiments performed by Pitt [8].

Example numerical solutions for h, u and G with $\Delta x = 400/(100 \times 2^6) \approx 0.06m$ are plotted in Figure 2. These examples demonstrate that the numerical solutions reproduced the analytic solutions well.

The convergence properties of the method as Δx varies are given in Figure 3 over the whole domain using the L_2 norm (24) and just the error at the peak. The L_2 norm demonstrates that all quantities are approximated with second-order accuracy, and thus the method is fully second-order accurate. The error at the peak was measured by taking the relative difference between the numerical solutions value at the peak of the wave which are given by $\max(\boldsymbol{h}^n)$, $\max(\boldsymbol{u}^n)$ to the analytic values which are $a_0 + a_1$ and $ca_0/(a_0 + a_1)$ respectively. The error at the peak demonstrates that even with the slope limiting and the diffusion of the flux approximation [9], the numerical solutions reproduce the peak well with little diffusion.

The conservation error C_1 (25) of the numerical solutions as Δx varies is given in Figure 4. This conservation measure demonstrates that due to the use of the finite volume method h and G are conserved up to round-off error, which increases as Δx increases. Since uh and $\mathcal{E}$ are not the conserved quantities in our finite volume

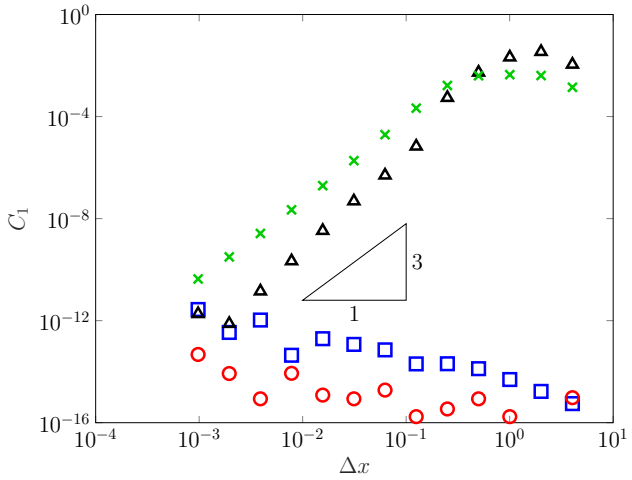

Figure 4: Conservation plot for h (□) , G (○), uh (△) and $\mathcal{E}$ (×) as Δx varies.

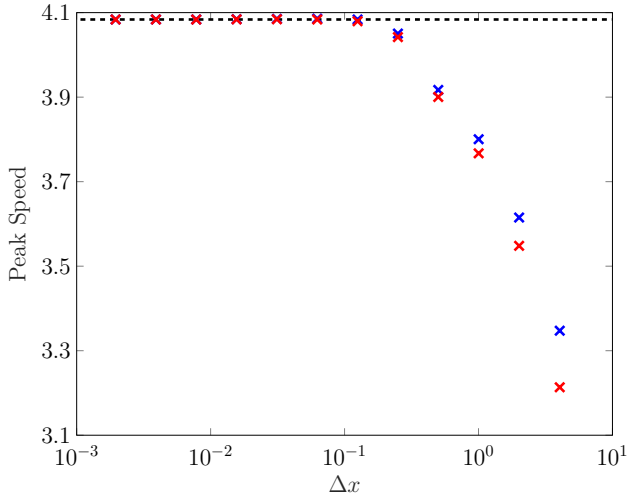

Figure 5: Plot of S_{upper} (×), S_{lower} (×) and the analytic value c (– –) as Δx varies.

based method, they are not conserved up to round-off error as can be seen. However, the conservation properties of uh and $\mathcal{E}$ are still good, and actually better than expected with both exhibiting conservation errors that have better than second-order convergence in Δx.

By locating the cell on which $\boldsymbol{h}^n$ achieves its maximum, we can provide an upper and lower bound for the speed of the numerical solution to the travelling wave problem where the lower bound is $S_{\text{lower}} = (x_{\text{peak cell}} - 0.5\Delta x)/t$ and the upper bound is $S_{\text{upper}} = (x_{\text{peak cell}} + 0.5\Delta x)/t$. These upper and lower bounds are compared to the analytic value c in Figure 5. This figure demonstrates the diffusion of the numerical scheme, as when Δx is large, both the upper and lower bounds on the wave speed are below the analytic value. However, this diffusion becomes negligible when Δx is small, and for the lowest Δx value we actually have $S_{\text{lower}} < c < S_{\text{upper}}$, indicating that the peak of the wave is located in the expected cell at the final time.

These results agree well with the numerical solutions of Pitt [8], who compared various numerical methods for the SGN equations. Additionally these added measures further justify the use of finite volume based methods for solving water wave equations with dispersion.

5.2.2. SWWE ($\beta_1 = \beta_2 = 0$) - Dam-break Solution

When $\beta_1 = \beta_2 = 0$ the gSGN equations reduce to the SWWE which have an analytic solution to the dam-break problem given by the initial conditions

$$h(x,0) = \begin{cases} h_0 & x < 0 \\ h_1 & x \geq 0 \end{cases} \tag{27}$$

$$u(x,0) = 0 \tag{28}$$

$$G(x,0) = 0. \tag{29}$$

The solution to the dam-break problem is given by

$$h(x,t) = \begin{cases} h_0 & , \quad x \leq -t\sqrt{gh_0} \\ \frac{4}{9g}\left(\sqrt{gh_0} - \frac{x}{2t}\right)^2 & , \quad -t\sqrt{gh_0} < x \leq t\left(u_2 - \sqrt{gh_2}\right) \\ h_2 & , \quad t\left(u_2 - \sqrt{gh_2}\right) < x \leq tS_2 \\ h_1 & , \quad tS_2 \leq x \end{cases} \tag{30}$$

$$u(x,t) = \begin{cases} 0 & , \quad x \leq -t\sqrt{gh_0} \\ \frac{2}{3}\left(\sqrt{gh_0} + \frac{x}{t}\right) & , \quad -t\sqrt{gh_0} < x \leq t\left(u_2 - \sqrt{gh_2}\right) \\ u_2 & , \quad t\left(u_2 - \sqrt{gh_2}\right) < x \leq tS_2 \\ 0 & , \quad tS_2 \leq x \end{cases}. \tag{31}$$

The constant state values h_2 and u_2 and the shock speed S_2 can be calculated for any initial conditions by solving

$$h_2 = \frac{h_0}{2}\left(\sqrt{1 + 8\left(\frac{2h_2}{h_2 - h_0}\left(\frac{\sqrt{gh_1} - \sqrt{gh_2}}{\sqrt{gh_0}}\right)\right)^2} - 1\right) \tag{32}$$

$$u_2 = 2\left(\sqrt{gh_1} - \sqrt{gh_2}\right), \tag{33}$$

$$S_2 = \frac{2h_2}{h_2 - h_1}\left(\sqrt{gh_0} - \sqrt{gh_2}\right). \tag{34}$$

The initial conditions as well as the analytic solution are discontinuous. Due to the discontinuities the solutions to the initial conditions are not unique, as solving any pair of the 3 conservation equations (1), gives solutions with similar structures but different constant values. The solution presented above is solution of the mass and momentum equations, as these equations are the basis of the numerical method.

A number of numerical experiments were run for the dam-break problem with $h_0 = 2m$ and $h_1 = 1m$. The domain of the solution was $[-250, 250]$ with a final time of $t = 35s$. The spatial resolution was varied like so $\Delta x = 500/(100 \times 2^l)$ where l was increased from 0 to 12. To satisfy the CFL condition (23) the time step length $\Delta t = \Delta x / \left(2\sqrt{gh_0}\right)$ was used. The limiting parameter θ was set to be $\theta = 1.0$ and the acceleration due to gravity $g = 9.81 m^2/s$ was used.

Example numerical solutions with the spatial resolution $\Delta x = 500/(100 \times 2^5) \approx 0.15m$ and the analytic solutions for h, G and u at the final time are plotted in Figure 6. These figures demonstrate that the method is robust in the presence of steep gradients and accurately reproduces the analytic solution.

Figure 7 demonstrates the convergence of the solutions for h as Δx changes for the top of the rarefaction fan and the shock front. Since the bottom of the rarefaction fan is very similar to the top and the behaviour of the other quantities are produce similar plots these have been omitted. This figure demonstrates the convergence of the numerical solutions to the analytic solution as Δx decreases.

The presence of discontinuities in the analytic solution, make accurately assessing convergence of the numerical solutions difficult. To circumvent these issues, the convergence measure has been restricted to comparing the numerical and analytic solutions for the constant region between the rarefaction fan and the shock. This modified convergence measure as Δx varies is plotted in Figure 8a. This figure demonstrates that the scheme retains it's second-order accuracy away from discontinuities, as desired.

Since the analytic solution contains discontinuities all three conservation laws for h, G and $\mathcal{E}$ are not all satisfied simultaneously [10]. The result of this is that since we solved equations for h and G, these quantities

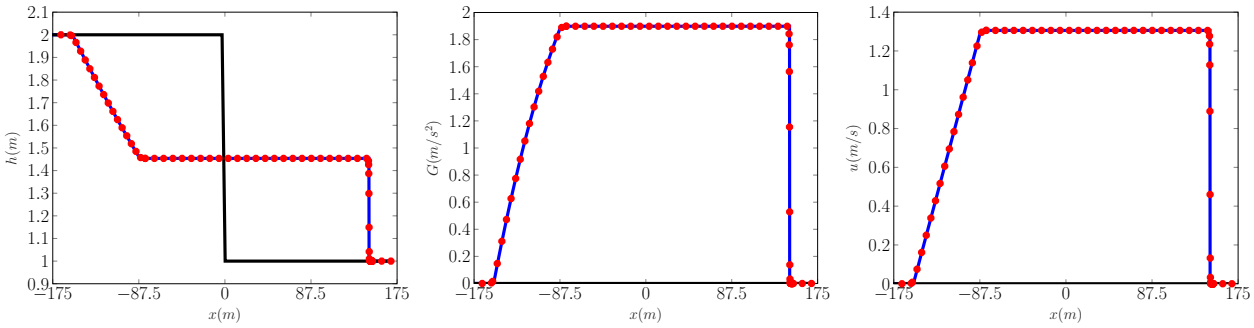

(a) h (b) $G = uh$ (c) u

Figure 6: Comparison of initial (—), analytic solution (—), and numerical solution with $\Delta x \approx 0.15m$ (●) at $t = 35s$.

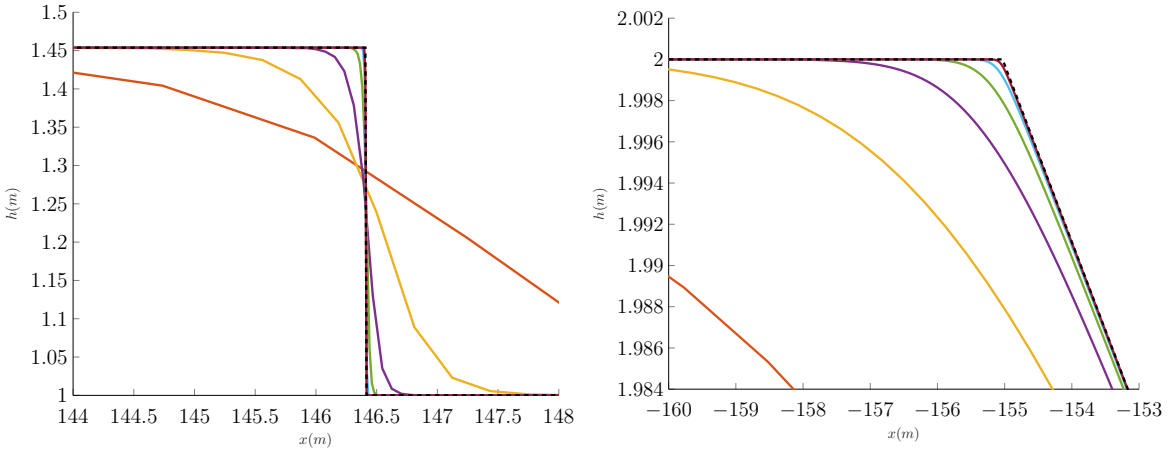

(a) Shock front (b) Top of rarefaction fan

Figure 7: Plots of h at $t = 35s$ for the smooth dam-break problem around important locations with $\Delta x = 5/2^2$ (—), $5/2^4$ (—), $5/2^6$ (—), $5/2^8$ (—), $5/2^{10}$ (—), $5/2^{12}$ (—) and the analytic solution (— —) of the SWWE to the corresponding dam-break problem.

File Name: gSGNpaper.tex
Date: 27/08/2020 at 12:55 Noon

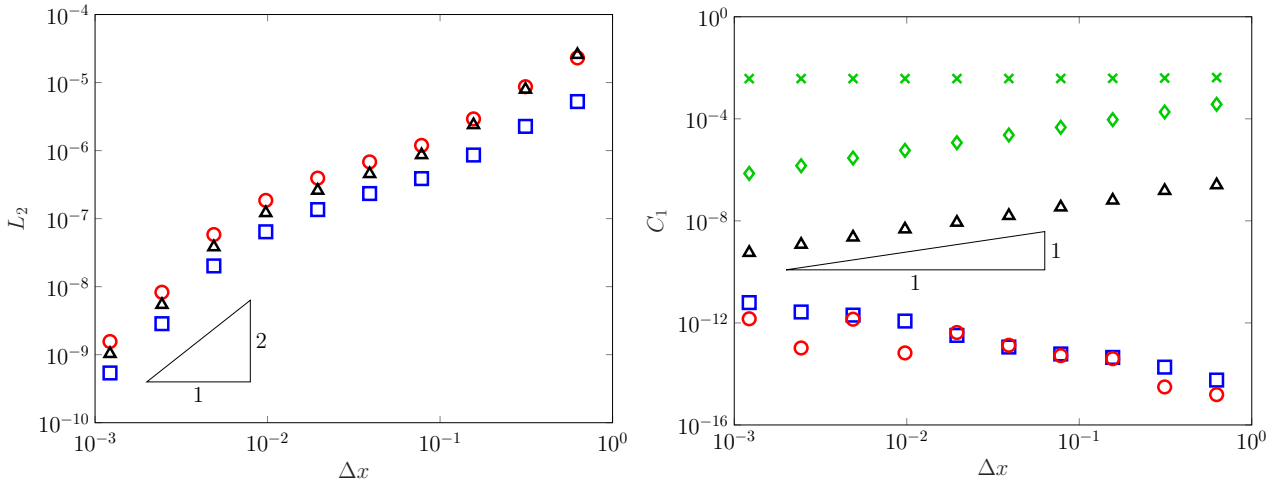

(a) L_2 for constant state with u (△)

(b) C_1 with uh (△)

Figure 8: Convergence and conservation plots for h (□) , G (○), $\mathcal{E}$ (×) and $\mathcal{E}^*$ (◇) as Δx varies.

are conserved in the analytic solutions however, $\mathcal{E}$ is no longer conserved and we actually lose energy as the shock propagates. I have taken account of the energy dissipation of the analytic solution by introducing a new measure $\mathcal{E}^*$ which measures the conservation error of the energy by comparing the total energy in the analytic solution at the final time and the numerical solution rather than the initial conditions. The conservation error for mass, momentum and energy as calculated normally and the new dissipated energy are all compared in Figure 8b. This figure demonstrates that due to the use of the finite volume method even in the presence of discontinuities the conserved quantities h and G are conserved up to round-off error, leading to their conservation error increasing as Δx increases. The conservation of uh now only improves with first-order accuracy this is because the reconstruction reduces to first-order accuracy in the presence of discontinuities. Energy is not conserved by the analytic solution, and this can be seen with the conservation error of $\mathcal{E}$ not improving as Δx decreases. However, when accounting for the lack of energy conservation as done with $\mathcal{E}^*$ then we are able to recover the first-order accuracy observed in the conservation of uh.

To further justify the ability of the method to resolve the discontinuous analytic solution, I have found lower and upper bounds for the shock speed in the numerical solution. For the lower bound this was accomplished by finding the first cell with $\bar{h}_j \leq h_1 + \frac{9}{10}(h_2 - h_1)$ at the final time which we call x_{lower}, and for the upper bound this was achieved by finding the first cell with $\bar{h}_j \leq h_1 + \frac{1}{10}(h_2 - h_1)$ denoted x_{upper}. Consequently, the lower bound for the shock speed $S_{\text{lower}} = x_{\text{lower}}/t$ and the upper bound for the shock speed $S_{\text{upper}} = x_{\text{lower}}/t$ were calculated and compared to the analytic value S_2 in Figure 9. This figure demonstrates that as Δx decreases the numerical solutions are better resolving the shock. Additionally it demonstrates that x_{lower} and x_{upper} do bound the true location of the shock as expected.

These results demonstrate that the analytic solution of the SWWE has been accurately reproduced by the numerical method.

5.3. Forced Solutions

There are no currently known analytic solutions to the gSGN equations for other β values. Hence, to demonstrate the validity and versatility of the method to solve the gSGN for other β values, forced solutions are necessary. It is vital for the gSGN equations in particular because for the β values tested above β_2 is zero, and thus the shown analytic solutions do not assess the numerical methods accuracy for the β_2 term.

To generate a forced solution the forced gSGN equations are considered

$$\frac{\partial h}{\partial t} + \frac{\partial (uh)}{\partial x} = \frac{\partial h^*}{\partial t} + \frac{\partial (u^* h^*)}{\partial x} \tag{35a}$$

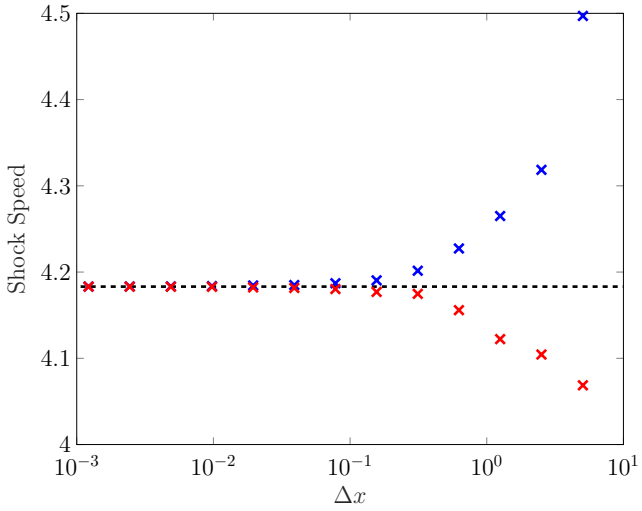

Figure 9: Plot of S_{upper} (×), S_{lower} (×) and S_2 (– –) as Δx varies.

$$\frac{\partial G}{\partial t} + \frac{\partial}{\partial x}\left(uG + \frac{gh^2}{2} - \beta_1 h^3 \frac{\partial u}{\partial x}\frac{\partial u}{\partial x} - \frac{1}{2}\beta_2 g h^2 \left[h\frac{\partial^2 h}{\partial x^2} + \frac{1}{2}\frac{\partial h}{\partial x}\frac{\partial h}{\partial x}\right]\right) =$$
$$\frac{\partial G^*}{\partial t} + \frac{\partial}{\partial x}\left(u^*G^* + \frac{g\left(h^*\right)^2}{2} - \beta_1\left(h^*\right)^3 \frac{\partial u^*}{\partial x}\frac{\partial u^*}{\partial x} - \frac{1}{2}\beta_2 g\left(h^*\right)^2 \left[h^*\frac{\partial^2 h^*}{\partial x^2} + \frac{1}{2}\frac{\partial h^*}{\partial x}\frac{\partial h^*}{\partial x}\right]\right). \quad (35b)$$

The forced gSGN admit the solutions h^*, u^* and G^* assuming G^* appropriately satisfies (7c). Since these equations are satisfied for any chosen h^*, u^* and G^* and any β values, forced solutions can be used to verify the method for a larger class of problems than permitted by currently known analytic solutions. In particular, problems were $\beta_2 \neq 0$ which were not covered in the above validation with analytic solutions. Since the left hand-side of these modified equations are approximated by the numerical method, combining the numerical method with the analytic expressions for the right hand-side, produces a method that approximates the forced gSGN equation (35) with the same convergence properties as the underlying numerical method for the gSGN equations.

The following forced solution

$$h^*(x,t) = a_0 + a_1 \exp\left(\frac{(x-a_2 t)^2}{2a_3}\right) \quad (36a)$$

$$u^*(x,t) = a_4 \exp\left(\frac{(x-a_2 t)^2}{2a_3}\right) \quad (36b)$$

$$\beta_1(x,t) = a_6 \quad (36c)$$
$$\beta_2(x,t) = a_7 \quad (36d)$$

where G^* is given by (7c), were used. These forced solutions describe Gaussian bumps in h and u that travel at a constant speed a_2. This forced solution was chosen because it is smooth and also none of the terms in (35) are constant over the whole domain. Smoothness is necessary for the current description of the forced solutions, since it requires the derivatives to be defined in the classical strong sense. While the last point ensures that we haven't picked a problem that is too simple, and thus doesn't require accurately modelling all the terms in (35). This ensures that the forced solutions are assessing the whole numerical method.

The particular parameter values $a_0 = 1$, $a_1 = 0.5$, $a_3 = 20$ and $a_4 = 0.3$ were chosen in this investigation, while multiple β values were tested we will be focusing on $a_6 = 2/15 + 2/3$ and $a_7 = 2/15$ below.

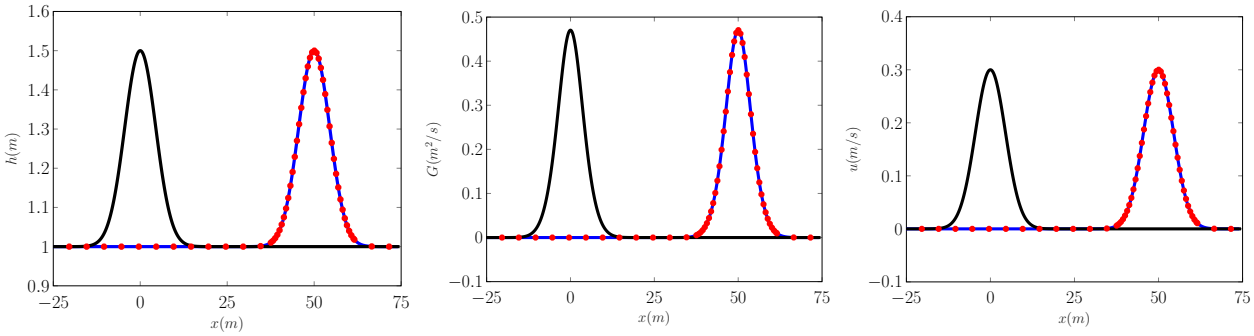

(a) h (b) G (c) u

Figure 10: Example plots Initial (—), analytic solution (—), and numerical solution with $\Delta x \approx 0.06m$ (●).

The numerical solutions were produced over the domain $[-100, 100]$ with a final time of $t = 10$. The spatial resolution was varied like so $\Delta x = 200/(100 \times 2^l)$, while the CFL condition was satisfied by setting $\Delta t = \Delta x / \left(2\left[a_4 + a_2 + \sqrt{g\left(a_0 + a_1\right)}\right]\right)$. The acceleration due to gravity $g = 9.81 m^2/s$ was used.

For the forced solutions the limiting on the reconstruction on h, u and G was removed. Firstly, because these forced solutions are smooth, such reconstruction is not necessary. Secondly, because when the slope limiting is included errors at the peak of the Gaussian bump are produced due to the change in finite difference stencils and the setting of the slope to zero when one of the finite difference approximations is zero or a different sign. These errors pollute the errors of the underlying numerical method and so to remove them the limiting was removed. This error pollution from the limiting is not observed for the analytic solution of the SGN equations, or forced solutions with $\beta_2 = 0$. Therefore, it seems that the numerical approximation to the β_2 term is highly sensitive to the limiting.

Figure 10 compares an example numerical solution at the final time for h, G and u with $\Delta x = 200/(100 \times 2^5) \approx 0.06$ with the analytic solution. These example solutions demonstrate that the numerical method is able to reproduce the forced solution well, validating the numerical methods approximation to all terms in (7).

Figure 11 demonstrates the convergence of the numerical scheme as Δx decreases. All quantities of interest are converging at the expected second-order. Since the RHS is given analytically, the observed error is caused by the numerical method. Therefore, these results demonstrate that the scheme is second-order for all terms in gSGN equations. Unfortunately as stated above, to accurately reproduce the forced solutions and achieve the theoretical accuracy the reconstruction limiting had to be removed. Therefore, these forced solutions only validate the method without this limiting. However, given that the limiting only affects extrema and discontinuities this study is sufficient to justify the example numerical method and thus the proposed numerical scheme for the gSGN equations.

6. Conclusion

A modified version of the numerical scheme for the SGN outlined by Zoppou et al. [7] was used to solved the gSGN equations [4, 1]. This numerical scheme for the gSGN was validated by describing a fully second-order order implementation as an example numerical method. This example numerical method was validated against analytic solutions of the SGN and SWWE equations and forced solutions. The analytic solutions demonstrate that the gSGN solver accurately reproduces important members of the gSGN family of equations whilst conserving the quantities of interest, and the forced solutions demonstrate that the method remains second-order for all values of the free parameters, β_1 and β_2. The gSGN method described above is the first well validated numerical method for the gSGN equations

[1] D. Clamond and D. Dutykh. Non-dispersive conservative regularisation of nonlinear shallow water (and isentropic euler equations). *Communications in Nonlinear Science and Numerical Simulation*, 55:237–247, 2018.

[2] F. Serre. Contribtion à l'étude des écoulements permanents et variables dans les canaux. *La Houille Blanche*, 6:830–872, 1953.

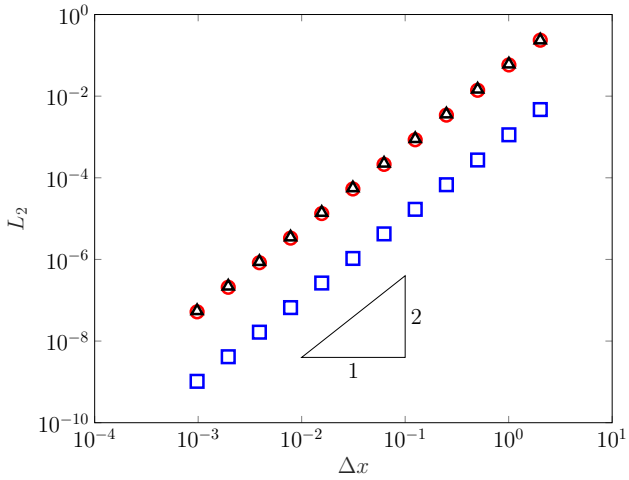

Figure 11: Convergence plot of h (□) , G (○), u (△) for the forced solutions for various Δx values.

[3] G. B. Whitham. Non-linear dispersion of water waves. *Journal of Fluid Mechanics*, 27(2):399412, 1967.

[4] D. Clamond, D. Dutykh, and D. Mitsotakis. Conservative modified Serre-Green-Naghdi equations with improved dispersion characteristics. *Communications in Nonlinear Science and Numerical Simulation*, 45: 245–257, 2017.

[5] C. Zoppou. *Numerical Solution of the One-dimensional and Cylindrical Serre Equations for Rapidly Varying Free Surface Flows*. PhD thesis, Australian National University, Mathematical Sciences Institute, College of Physical and Mathematical Sciences, Australian National University, Canberra, ACT 2600, Australia, 2014.

[6] C. Zoppou, S.G Roberts, and J. Pitt. A solution of the conservation law form of the serre equations. *The Australia and New Zealand Industrial and Applied Mathematics Journal*, 57(4):385–394, 2016.

[7] C. Zoppou, J. Pitt, and S. Roberts. Numerical solution of the fully non-linear weakly dispersive Serre equations for steep gradient flows. *Applied Mathematical Modelling*, 48:70–95, 2017.

[8] J.P.A. Pitt. *Simulation of Rapidly Varying and Dry Bed Flow using the Serre equations solved by a Finite Element Volume Method*. PhD thesis, Australian National University, Mathematical Sciences Institute, College of Physical and Mathematical Sciences, Australian National University, Canberra, ACT 2600, Australia, 2019.

[9] J.P.A. Pitt, C. Zoppou, and S.G. Roberts. Behaviour of the Serre equations in the presence of steep gradients revisited. *Wave Motion*, 76(1):61–77, 2018.

[10] Y. Pu, R.L. Pego, D. Dutykh, and D. Clamond. Weakly singular shock profiles for a non-dispersive regularization of shallow-water equations. *Communications in Mathematical Sciences*, 16:1361–1378, 2018.

[11] A. G. Filippini, M. Kazolea, and M. Ricchiuto. A flexible genuinely nonlinear approach for nonlinear wave propagation, breaking and run-up. *Journal of Computational Physics*, 310:381–417, 2016.

[12] J.S.A. do Carmo, J.A. Ferreira, and L. Pinto. On the accurate simulation of nearshore and dam break problems involving dispersive breaking waves. *Wave Motion*, 85:125 – 143, 2019.

[13] O. Le Métayer, S. Gavrilyuk, and S. Hank. A numerical scheme for the Green-Naghdi model. *Journal of Computational Physics*, 229(6):2034–2045, 2010.

[14] A. Kurganov, S. Noelle, and G. Petrova. Semidiscrete central-upwind schemes for hyperbolic conservation laws and Hamilton-Jacobi equations. *Journal of Scientific Computing, Society for Industrial and Applied Mathematics*, 23(3):707–740, 2002.

[15] M. Li, P. Guyenne, F. Li, and L. Xu. High order well-balanced CDG-FE methods for shallow water waves by a Green-Naghdi model. *Journal of Computational Physics*, 257(1):169–192, 2014.

[16] S. Gottlieb, C. Shu, and E. Tadmor. Strong stability-preserving high-order time discretization methods. *Review, Society for Industrial and Applied Mathematics*, 43(1):89–112, 2001.

[17] S. Roberts and C. Zoppou. Explicit schemes for dam-break simulations. *Journal of Hydraulic Engineering*, 129:11–34, 2003.

[18] S.D. Conte and C. De Boor. *Elementary numerical analysis: An algorithmic approach.* International Series in Pure and Applied Mathematics. McGraw-Hill Inc., New York, 3rd edition, 1980.

[19] R. Courant, K. Friedrichs, and H. Lewy. On the partial difference equations of mathematical physics. *IBM Journal of Research and Development*, 11(2):215–234, 1967.

[20] G.A. El, R.H.J. Grimshaw, and N.F. Smyth. Unsteady undular bores in fully nonlinear shallow-water theory. *Physics of Fluids*, 18(2):027104, 2006.